



A specific aggregation-induced emission-conjugated polymer enables visual monitoring of osteogenic differentiation

Zhenyu Zheng^{a,1}, Taotao Zhou^{b,1}, Rong Hu^{b,1}, Minjun Huang^a, Xiang Ao^a, Jun Chu^a, Tao Jiang^a, Anjun Qin^{b,*,**}, Zhongmin Zhang^{a,*}

^a Department of Orthopaedics, The Third Affiliated Hospital, Southern Medical University, Academy of Orthopaedics, Guangdong Province, Guangzhou, 510630, China

^b State Key Laboratory of Luminescent Materials and Devices, Guangdong Provincial Key Laboratory of Luminescence from Molecular Aggregates, Center for Aggregation-Induced Emission, South China University of Technology, Guangzhou, 510640, China

ARTICLE INFO

Keywords:

Osteogenic differentiation
Osteoblasts
Aggregation-induced emission
Fluorescence
Calcium ions

ABSTRACT

Osteogenic differentiation is the basis of bone growth and repair related to many diseases, in which evaluating the degree and ability of osteogenic transformation is quite important and highly desirable. However, fixing or stopping the growth of cells is required for conventional methods to monitor osteogenic differentiation, which cannot realize the full investigation of the dynamic process. Herein, a new anion conjugated polymer featuring aggregation-induced emission (AIE) characteristics is developed with excellent solubility for *in-situ* monitoring the process of osteogenic differentiation. This novel polymer can bind with osteogenic differentiated cells, and the intracellular fluorescence increases gradually with the enhancement of osteogenic differentiation. Moreover, it possesses good biosafety with negligible effect on cell activity and osteogenic differentiation, which cannot be realized by the typical method of Alizarin Red S staining. Further study shows that the polymer crosses the cell membrane through endocytosis and enriches in lysosomes, whereas no obvious fluorescence is detected with other cells, including non-differentiated osteoblast cells, under the same conditions, demonstrating the high selectivity. This is the first fluorescent probe with excellent specificity to realize real-time observation of the process of osteogenic differentiation. Therefore, PTB-EDTA shows great promise in the study of osteogenic differentiation and related applications.

1. Introduction

Nonunion and delayed union remain a major complication of bone fractures, which is a great burden to both patients and healthcare systems [1]. Osteogenic differentiation is a complex physiological process and modulated by various factors [2,3]. Osteoblasts play an important role in maintaining the balance of bone metabolism, in which fracture healing is highly dependent on the activity of osteoblasts proliferation and differentiation. Thus, the detection and evaluation of the degree of osteogenic differentiation is quite important in orthopedic and related diseases. During osteogenic differentiation, collagen-enriched extracellular matrix (ECM) is formed [4], and calcium ions (Ca²⁺) and inorganic phosphate accumulate to form hydroxyapatite crystals [5–7]. Matrix mineralization in cell cultures is the most important indicator of osteogenic differentiation. Many biochemical analysis methods such as

immunostaining, quantitative real-time polymerase chain reaction (RT-qPCR) and protein blotting assays have been developed to observe the degree of osteogenic differentiation in clinic and scientific research [8–11]. Among these strategies, the quantification of mineralization based on Alizarin Red S staining is the most common method [5,12]. However, monitoring the dynamics of osteogenic differentiation is not easy to realize because cell fixation and other multiple staining steps are required in the majority of strategies [13]. Most importantly, the detection method does not discern the osteogenic differentiation ability of the cell itself. Given to the high sensitivity and easy operation, fluorescent probes have also been developed for the detection of biomarker, such as MMP13 and ALP, to detect the osteogenic differentiation [14–16]. Nevertheless, the evaluation of the degree of osteogenic differentiation is not easy to realize based on these strategies. Thus, it is urgent for non-invasive strategies to detect osteogenic differentiation

Peer review under responsibility of KeAi Communications Co., Ltd.

* Corresponding author.

** Corresponding author.

E-mail addresses: msqinaj@scut.edu.cn (A. Qin), zmmzcc@smu.edu.cn (Z. Zhang).

¹ These authors contributed equally to this work.

<https://doi.org/10.1016/j.bioactmat.2020.06.020>

Received 8 April 2020; Received in revised form 10 June 2020; Accepted 28 June 2020

2452-199X/© 2020 The Authors. Publishing services by Elsevier B.V. on behalf of KeAi Communications Co., Ltd. This is an open access article under the CC BY-NC-ND license (<http://creativecommons.org/licenses/by-nc-nd/4.0/>).

with high sensitivity for dynamic monitoring and early diagnosis.

Methods based on fluorescence detection have been developed because of its high sensitivity and excellent repeatability. However, conventional fluorescent probes are highly emissive in solutions but their emission mostly decreased or is totally quenched in the aggregate and solid states, that is, they undergo aggregation-caused quenching (ACQ) effect, which will reduce the sensitivity since the aggregation is a spontaneous process in physiological environments [17,18]. Thus, the ACQ effect has limited their wide applications in related fields, especially in the early sensing applications. Exactly opposite to the ACQ effect, fluorescent materials with aggregation-induced emission (AIE) features, which can positively utilize the natural aggregation process, display stronger emission in the aggregate and solid states than that in the solution state, facilitating the development of fluorescent probes with high sensitivity and selectivity in real applications [19]. Moreover, AIE probes generally possess large Stokes shift and excellent photostability, making them desirable for sensing and visualization applications. Indeed, they have been widely used in bioimaging and sensing areas [20–26].

Herein, to overcome the limitations of typical methods and enable live analyses, we developed a new type of fluorescent probe, *i.e.* an AIE-active tetraphenylthene (TPE) and benzothiadiazole containing conjugated polymer with ethylenediaminetetraacetic acid moiety (PTB-EDTA) as its side-chains, for selective discrimination of osteoblasts and *in-situ* monitoring the osteogenic differentiation process (Fig. 1A).

Previously reported AIE-active polymer with similar structure shows great selectivity towards microbes over mammalian cells for bacterial eradication [27]. This polymer not only possesses excellent solubility and biocompatibility but also shows high affinity towards Ca^{2+} by chelation interaction via EDTA groups. Given that the increasing demand of Ca^{2+} during osteogenic differentiation [28,29], PTB-EDTA could cross the cell membrane through endocytosis by effective Ca^{2+} chelation, resulting in selective enrichment in osteoblasts, which could not be realized by its monomer (MTB-EDTA) (Fig. S5). Notably, the detection of osteogenic differentiation based on PTB-EDTA is more sensitive than that of Alizarin Red S staining. Moreover, PTB-EDTA has a negligible effect on the osteogenic process compared to traditional methods. Thus, this novel PTB-EDTA polymer has great significance for the rapid and real-time identification of the degree of osteogenic differentiation.

2. Material and methods

2.1. Equipment

^1H and ^{13}C NMR spectra were measured on a Bruker AV 500 spectrometer in appropriated deuterated solution at room temperature. UV-vis absorption spectra were measured on a Shimadzu UV-2600 spectrophotometer. Photoluminescence spectra were recorded on a Horiba Fluoromax-4 spectrofluorometer. Solution fluorescence

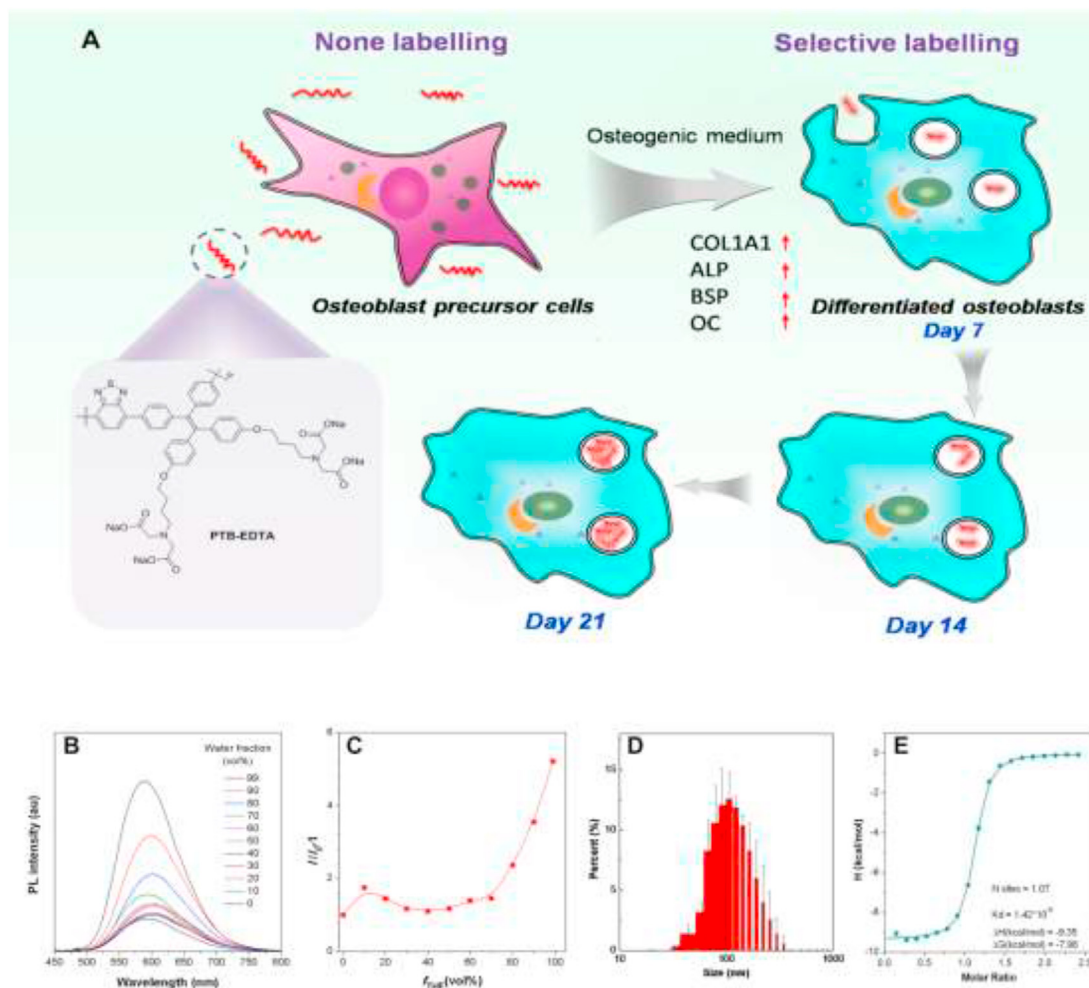


Fig. 1. (A) The chemical structures and cartoon illustration of the high lysosomal accumulation of PTB-EDTA followed by the cellular internalization. (B) Fluorescence emission spectra of PTB-EDTA in H₂O-THF solution of different proportions, $\lambda_{\text{ex}} = 429$ nm. (C) The fluorescence intensity ratio curve of PTB-EDTA in H₂O-THF solution of different proportions, $\lambda_{\text{ex}} = 429$ nm. (D) The particle size distribution of PTB-EDTA in water. PTB-EDTA = 10^{-5} M. (E) The enthalpy of the system varies with the molar ratio between CaCl_2 and PTB-EDTA.

quantum yields were measured using a Hamamatsu absolute PL quantum yield spectrometer C11347 Quantaury-QY. Zeta potential measurements were conducted on dynamic light scattering (Malvern ZSE, UK). Isothermal titration calorimetry (ITC) was conducted on Malvern MicroCal ITC. Cells were observed under confocal laser-scanning microscope (CLSM) (LSM710, Zeiss, Germany).

2.2. Synthesis of compounds and polymer

4,4'-(2,2-bis(4-(4-bromobutoxy)phenyl)ethene-1,1-diyl)bis(bromobenzene) (3): Compound 2 (7.5 g, 35 mmol) and K_2CO_3 (4.8 g, 35 mmol) were added to a 100 mL two-necked flask, dissolved in 40 mL of acetone. Compound 1 (3.65 g, 7 mmol) dissolving in 20 mL of acetone was gradually added, and the reaction mixture was heated to reflux for 12 h under N_2 . After cooling to room temperature, acetone was distilled off under reduced pressure. 20 mL of deionized water and dichloromethane were added to dissolve the solid, then the mixture was extracted for three times with 20 mL of dichloromethane. The combined organic phase was washed for three times with deionized water. Drying over $MgSO_4$, the solvent was removed, and the residue was purified by silica-gel column chromatography using hexane/dichloromethane (2:1) as eluent. White solid of Compound 3 was obtained in 70% yield (Scheme S1A). 1H NMR (500 MHz, $CDCl_3$): δ 7.22 (d, $J = 10$ Hz, 4H), δ 6.87 (m, 8H), δ 6.63 (d, $J = 10$ Hz, 4H), δ 3.94 (t, $J = 5$ Hz, 4H), δ 3.48 (t, $J = 10$ Hz, 4H), δ 2.06 (m, 4H), δ 1.91 (m, 4H); ^{13}C NMR (125 MHz, $CDCl_3$): δ 157.69, 142.75, 141.42, 136.57, 135.62, 132.97, 132.50, 130.99, 120.27, 113.70, 66.64, 33.46, 29.45, 27.87.

Tetraethyl 2,2',2'',2'''-(((2,2-bis(4-bromophenyl)ethene-1,1-diyl)bis(4,1-phenylene))bis(oxy))bis(butane-4,1-diyl)bis(azanetriyl)tetraacetate (5): Compound 3 (792 mg, 1 mmol) and $NaHCO_3$ (700 mg, 4 mmol) were added to a 50 mL two-necked flask with the addition of 20 mL DMF, and Compound 4 (1.89 g, 10 mmol) was gradually added. The reaction mixture was heated to 60 °C for 12 h under N_2 . After cooling to room temperature, 20 mL of deionized water and Ethyl acetate (EA) were added, then the mixture was extracted for three times with 20 mL of EA. The combined organic phase was washed for three times with deionized water. Drying over $MgSO_4$, the solvent was removed, and the residue was purified by silica-gel column chromatography using hexane/Ethyl acetate (2:1) as eluent. Yellow sticky of Compound 5 was obtained in 47% yield (Scheme S1A). 1H NMR (500 MHz, $CDCl_3$): δ 7.22 (d, $J = 5$ Hz, 4H), δ 6.86 (t, $J = 10$ Hz, 8H), δ 6.62 (d, $J = 10$ Hz, 4H), δ 4.16 (t, $J = 10$ Hz, 8H), δ 3.90 (d, $J = 5$ Hz, 4H), δ 3.55 (m, 8H), δ 2.77 (t, $J = 10$ Hz, 4H), δ 1.78 (t, $J = 5$ Hz, 4H), δ 1.64 (t, $J = 5$ Hz, 4H), δ 1.26 (t, $J = 5$ Hz, 12H); ^{13}C NMR (125 MHz, $CDCl_3$): 171.34, 157.81, 150.51, 133.24, 132.76, 131.85, 130.95, 128.53, 127.63, 113.69, 67.74, 60.47, 56.45, 55.01, 53.97, 45.47, 27.59, 26.88, 24.53, 14.26.

Polymer 8: Compound 6 (100.8 mg, 0.1 mmol), Compound 7 (38.8 mg, 0.1 mmol) and $Pd(PPh_3)_4$ (10 mg, 0.0086 mmol), K_2CO_3 (276 mg, 2 mmol) were added to a round-bottomed flask. A mixture of toluene (1 mL) and H_2O (1 mL) was added to the flask, and the reaction mixture was heated to 80 °C for 24 h under N_2 . After cooling to room temperature, 10 mL of deionized water and EA were added, then the mixture was extracted for three times with 10 mL of EA. The combined organic phase was washed for three times with deionized water. The polymer was filtered by cotton and precipitated in hexane, and then dried under vacuum for 24 h to afford the neutral Polymers 8 as an orange solid in 71% yield (Scheme S1A). 1H NMR (500 MHz, $CDCl_3$): δ 7.74–7.82 (m, 4H), δ 7.24–7.27 (m, 4H), δ 7.14 (d, $J = 10$ Hz, 1H), δ 6.92–7.04 (m, 5H), δ 6.65 (t, $J = 10$ Hz, 4H), δ 4.13–4.17 (m, 8H), δ 3.90 (t, $J = 5$ Hz, 4H), δ 3.52–3.55 (m, 4H), δ 2.74–2.77 (m, 4H), δ 1.63–1.77 (m, 8H), 1.22–1.28 (m, 12H).

PTB-EDTA: Polymer 8 (50 mg, 0.05 mmol), $NaOH$ (1.2 g, 30 mmol) was added to a round-bottomed flask, then a mixture of THF (1 mL) and H_2O (1 mL) was added. The mixture was stirred at room temperature

for 12 h, after the addition of the dilute hydrochloric acid to adjust the pH to weakly alkaline, the crude reaction mixture were purified by dialysis (molecular weight cutoff = 3600), then freeze-dried under vacuum to obtain PTB-EDTA as an orange solid in 76% yield.

2.3. Isothermal titration microcalorimetry (ITC)

Calorimetric measurements were performed at 25.00 ± 0.01 °C on a Malvern MicroCal ITC microcalorimetric system. The cell was initially loaded with $0.3 \text{ mL} \times 10^{-4} \text{ M}$ PTB-EDTA, and then $2.5 \times 10^{-3} \text{ M}$ $CaCl_2$ solution was injected into the stirred sample cell in portions of 4 μL until the desired concentration range had been covered. The observed enthalpy values (ΔH_{obs}) were obtained from the areas of the calorimetric peaks after titrations. The reference cell was filled with 300 μL buffer solutions.

2.4. Cell culture and differentiation

MC3T3-E1 subclone 14 cells, CNE2 cells, HCC827 cells, and HLF cells were purchased from Cell Bank of the Chinese Academy of Sciences (Shanghai, China). The cells were incubated with α -MEM with 10% fetal bovine serum (FBS) and 1% penicillin-streptomycin solution (Gibco, Grand Island, NY) at 37 °C with 5% CO_2 . The medium for osteogenic differentiation was α -MEM with 10% FBS supplemented with 10 mM β -glycerophosphate salt hydrate (G9422-10G, SIGMA, USA) and 50 mg/mL ascorbic acid (A800295, Macklin, China). MC3T3-E1 cells were seeded at a density of 1×10^5 cells/mL in confocal dish. Every 2 days the medium was replaced. To study the relationship of Ca^{2+} in the uptake of PTB-EDTA, cells after 14 days of osteogenic differentiation were washed with Ca^{2+} free MEM medium (11380037, Gibco, USA) for three times and incubated with the medium supplemented with PTB-EDTA for 6 h, sequentially. The control group were incubated with normal MEM medium (12492013, Gibco, USA) supplemented with PTB-EDTA for 6 h.

2.5. Evaluation of cytotoxicity

MC3T3-E1 cells were seeded in 96-well plates at a density of 1×10^4 cells/mL. After 24 h of culture, cells were treated with PTB-EDTA at the concentrations of 1, 10, 20, and 40 μM for 3 days. Then 20 μL of MTT (5 mg/mL) was added into each well, and incubated for 4 h. After removing the medium by aspiration, 100 μL of dimethyl sulfoxide (DMSO) was added to dissolve the formazan crystals for 10 min. The absorbance at 570 nm was measured by microplate reader (Synergy HTX, USA), and the survival rate of the cells was calculated by the proportion of absorbance value of each group. Normalize the absolute MTT values by scaling to the mean of cultures which have not been treated with PTB-EDTA.

2.6. Alizarin Red S staining and quantitative analysis

For Alizarin Red S staining, MC3T3-E1 cells were seeded in 6-well plates at a density of 1×10^5 cells/well and cultured in α -MEM. 3 days later, the medium was replaced with osteogenic medium. Alizarin Red S staining was performed at days 7, 14, and 21 after osteogenic differentiation. Cells were fixed in 4% paraformaldehyde for 15 min and washed twice with deionized water. 1 mL of Alizarin Red S solution (DS0101, LEAGENE, China) was added to each well for 30 min, and washed with deionized water before imaging. For quantitative analysis of calcium, 1 mL of 1% cetylpyridinium chloride (C129534, aladdin, China) was added into each well. After the mineralized nodules dissolved, 200 μL solution was taken out of each well and transferred to a 96-well plate. The absorbance value (OD value) was detected by microplate reader at the wavelength of 590 nm.

2.7. RT-qPCR assay

Total RNA was extracted from cells with TRIzol reagent (Life Technologies, Grand Island, NY, USA) according to the manufacturer's instructions. The purity and concentration of total RNA were determined with NanoVue Plus spectrophotometer. cDNA was synthesized with the PrimeScript™ RT Master Mix (Takara, Japan). RT-qPCR reactions were performed with TB Green™ Premix Ex Taq™ (Takara, Japan) according to the manufacturer's instructions. Beta-actin mRNA was used as the internal control for normalization and the $2^{-\Delta\Delta Ct}$ method were used to calculate the fold change. The primers purchased from Sangon Biotech Co., Ltd are provided in Table S2.

2.8. Endocytosis inhibitors and lysosomal imaging

In the energy-dependent endocytosis analysis, the cell was thermoregulated at 4 °C, under which condition energy-dependent endocytosis is inhibited. For the analysis of the endocytosis pathways by pharmacological inhibitors, cells were pre-treated with 5 µg/mL Chlorpromazine (Sigma) for 30 min or 100 µM Dynasore (Sigma) for 1 h. In the control group, the culture medium containing 0.1% DMSO was pretreated for 1 h. All cells were washed three times before incubated with medium containing 10 µM of PTB-EDTA for 6 h. Cell lysosomal imaging was assessed by employing LysoTracker Red DND-99 (L7528, Invitrogen) according to the manufacturer's instructions.

2.9. Statistical analyses

Data are presented as mean ± SD. Statistical analyses of data were performed using SPSS 20.0 (SPSS, Chicago, IL, USA). All data are representative of at least three independent experiments. Differences between groups were analysed by unpaired *t*-test or One-way analysis of variance. *P* < 0.05 was considered statistically significant.

2.10. Dynamic light scattering measurements

PTB-EDTA was dissolved in H₂O with the final concentration of 10 µM. 1 mL of solution was used for the observation of diameter distribution and zeta potential on dynamic light scattering (DLS).

3. Results and discussion

3.1. Photophysical properties of PTB-EDTA

PTB-EDTA was prepared according to the synthetic route shown in Scheme S1A. The structures of the monomers and polymer were fully characterized by ¹H and ¹³C NMR spectroscopy and satisfactory data were obtained (Figs. S1 and S2). And the molecular weight was measured to be 6800 with the PDI value of 1.26. After confirming the structure of the polymer, we studied its photophysical properties. As shown in Table S1, PTB-EDTA shows maximal absorption and emission at 429 and 594 nm, respectively. The Stokes shift is as large as 165 nm, which is desirable for bioimaging and sensing applications. PTB-EDTA exhibits weak fluorescence intensity in water because of its excellent solubility, and the intramolecular motion will relax the energy of the excited state. By adding the poor solvent of tetrahydrofuran (THF) to the aqueous solution, the fluorescence of PTB-EDTA is clearly enhanced at high THF fraction (Fig. 1B and C), which is readily attributed to the restriction of intramolecular motion upon the formation of aggregates [30], and the fluorescence quantum yield of the aggregate state is subsequently increased 3.4 times compare to the solution state (Table S1), indicating its AIE activity.

Moreover, we used dynamic light scattering (DLS) to study the distribution of PTB-EDTA in deionized water. As shown in Fig. 1D, the particle size of PTB-EDTA mainly ranges at 60–200 nm with an average diameter 103 nm, indicating that the formation of nanoaggregate is

induced by the rigidity and hydrophobicity of the π -conjugated backbones. Furthermore, the surface potential of PTB-EDTA was measured as -27 mV (Fig. S3), which indicated that the nanoparticles had a negatively charged surface in the aggregate state.

To investigate the ability of PTB-EDTA to bind with Ca²⁺, an isothermal titration calorimetry (ITC) experiment was carried out by titrating CaCl₂ (2.5×10^{-3} M) solution into PTB-EDTA (2×10^{-4} M) solution. Fig. 1E shows the raw data plot of the heat change versus time for the titration process. A large amount of heat (4.5 µcal/s) is released at the beginning of the experiment, demonstrating that the binding of PTB-EDTA to Ca²⁺ is quite efficient. With the addition of CaCl₂ into the solution, the exotherm gradually decreases because PTB-EDTA is saturated by Ca²⁺ coordination. The binding constant of the reaction is obtained with *K_b* value of 7×10^5 M⁻¹. Moreover, the small enthalpy change ($\Delta H_{\text{obs}} = -9.25$ kcal/mol) and the Gibbs change ($\Delta G = -7.98$ kcal/mol) indicate that the interaction between PTB-EDTA and calcium ions is driven by electrostatic and chelation interaction. Additionally, the binding ratio is approximately one, which indicates that each Ca²⁺ can bind with two PTB-EDTA molecules. These results indicate the efficient chelation of PTB-EDTA with Ca²⁺. Moreover, after the chelation with Ca²⁺, the diameter distribution of PTB-EDTA in water was enlarged (Fig. S4A), which further demonstrated the successful binding of PTB-EDTA towards Ca²⁺. The absorbance and emission spectra were also observed after the addition of different concentration of Ca²⁺. As shown in Fig. S4B, after the addition of Ca²⁺, there is negligible change in absorbance spectra, indicating there is no variation of structure conformation of PTB-EDTA. While, obvious enhancement in emission is detected after the incubation with Ca²⁺ (Fig. S4C), which may be attributed to the formation of aggregate with the restriction of the intramolecular motion to realize the AIE process.

3.2. Cytotoxicity of PTB-EDTA and its effect on osteogenesis

In order to investigate the biosafety, we studied the cytotoxicity of PTB-EDTA, and the MC3T3-E1 mouse osteoblast precursor cell line was selected as a representative, because it is a well-characterized model for bone formation and can differentiate into mineralizing bone cells under specific physicochemical stimulation [31,32]. Compared with the blank group, the concentrations of PTB-EDTA ranging from 1 to 40 µM had no effect on the proliferation of MC3T3-E1 cells (Fig. 2A). In addition, in order to evaluate the impact on osteogenic differentiation, we further examined various osteogenic marker mRNAs by RT-qPCR. The results showed that PTB-EDTA neither increased the expression of osteogenic biomarkers in normal medium, nor decreased the expression of osteogenic biomarkers in osteogenic medium (Fig. 2B–E). Alizarin Red S staining was utilized to evaluate the effect of PTB-EDTA on the formation of mineralized nodules (Fig. 2F). Quantitative analysis of mineralized nodules by cetylpyridinium chloride showed that PTB-EDTA won't affect the formation of mineralized nodules, even those were cocultured for 21 days (Fig. 2G). These results indicate the great biosafe of PTB-EDTA.

3.3. Specificity of cellular imaging and the ability of PTB-EDTA to detect osteogenic differentiation

In order to explore the selectivity of PTB-EDTA towards osteogenically differentiated cells, we first investigated the imaging ability of PTB-EDTA with different cell lines, including undifferentiated MC3T3-E1 cells. Herein, human nasopharyngeal carcinoma (CNE2) cells, human lung adenocarcinoma (HCC827) cells, human lung fibroblast (HLF) cells and MC3T3-E1 cells were selected as the representatives, which were subjected to incubate with PTB-EDTA under the same conditions. As shown in Fig. 3, only strong fluorescence is detected in differentiated MC3T3-E1 cells, and no obvious fluorescence of PTB-EDTA is found in other cell lines (CNE2, HCC827 and HLF), even the MC3T3-E1 cells without differentiation. Therefore, PTB-EDTA shows

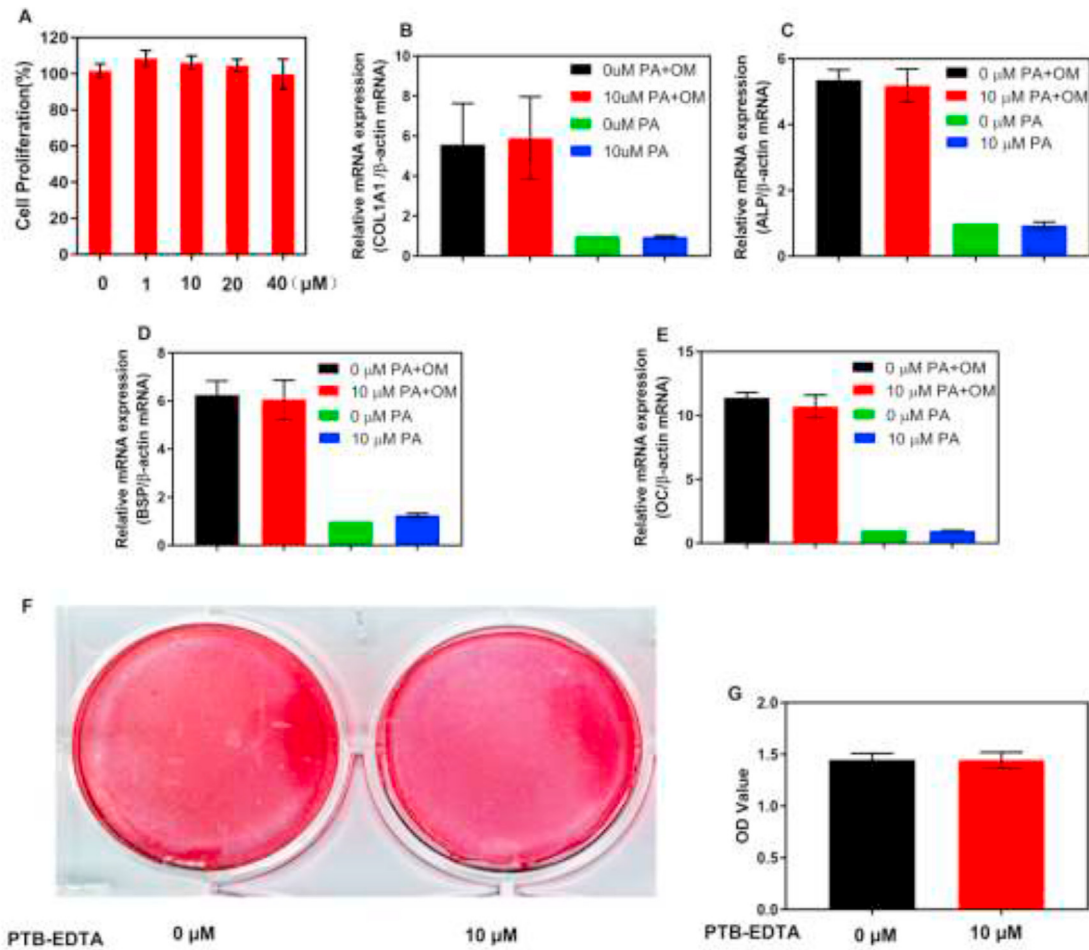


Fig. 2. The effect of PTB-EDTA on the process of osteogenic differentiation. (A) Cell viability was assessed using the MTT assay, M3T3-E1 cells were cultured with different concentrations of PTB-EDTA for 3 days. ($P = 0.18$). (B–E) MC3T3-E1 cells were incubated with PTB-EDTA for 14 days in osteogenic medium or normal medium. PTB-EDTA has no effect on the expression of COL1A1, ALP, BSP, and OC mRNA. ($P > 0.05$). (F) Representative photos of Alizarin Red S staining in M3T3-E1 cells incubated for 21 days in osteogenic medium with or without PTB-EDTA. (G) Quantitative analysis of mineralized nodules by cetylpyridinium chloride ($P = 0.93$). COL1A1 indicates collagen type 1 alpha 1; ALP, alkaline phosphatase; BSP, bone sialoprotein; OC, osteocalcin; OM, osteogenic medium; PA, PTB-EDTA. (For interpretation of the references to colour in this figure legend, the reader is referred to the Web version of this article.)

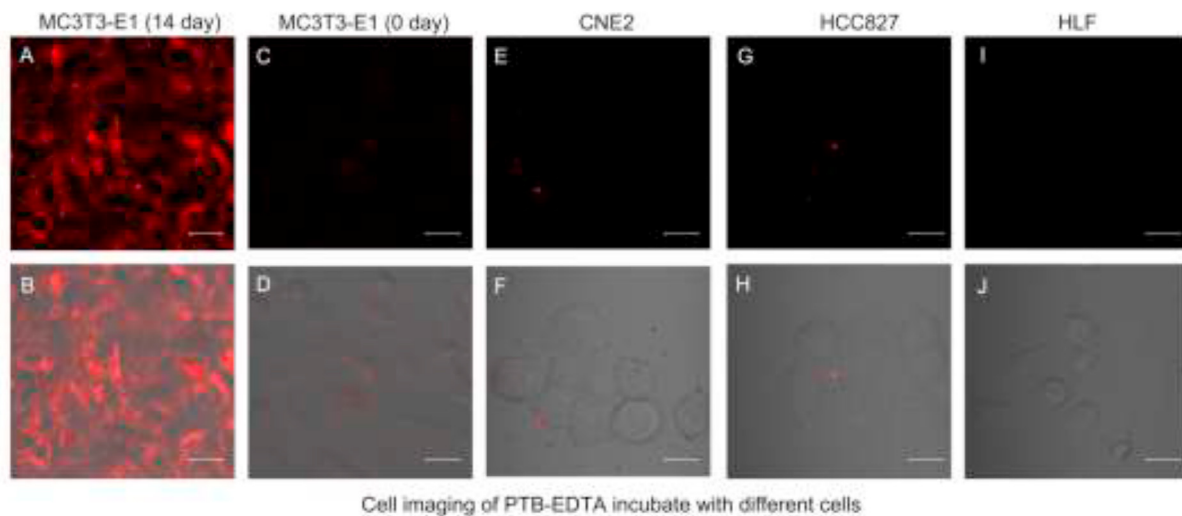


Fig. 3. The specific imaging of PTB-EDTA in osteogenic differentiation cells. Fluorescence and merged images of PTB-EDTA in differentiated MC3T3-E1 cells (A, B), MC3T3-E1 cells (C, D), CNE2 cells (E, F), HCC827 cells (G, H), and HLF cells (I, J) after incubation of 12 h. Scale bars = 20 μm. PTB-EDTA = 10 μM.

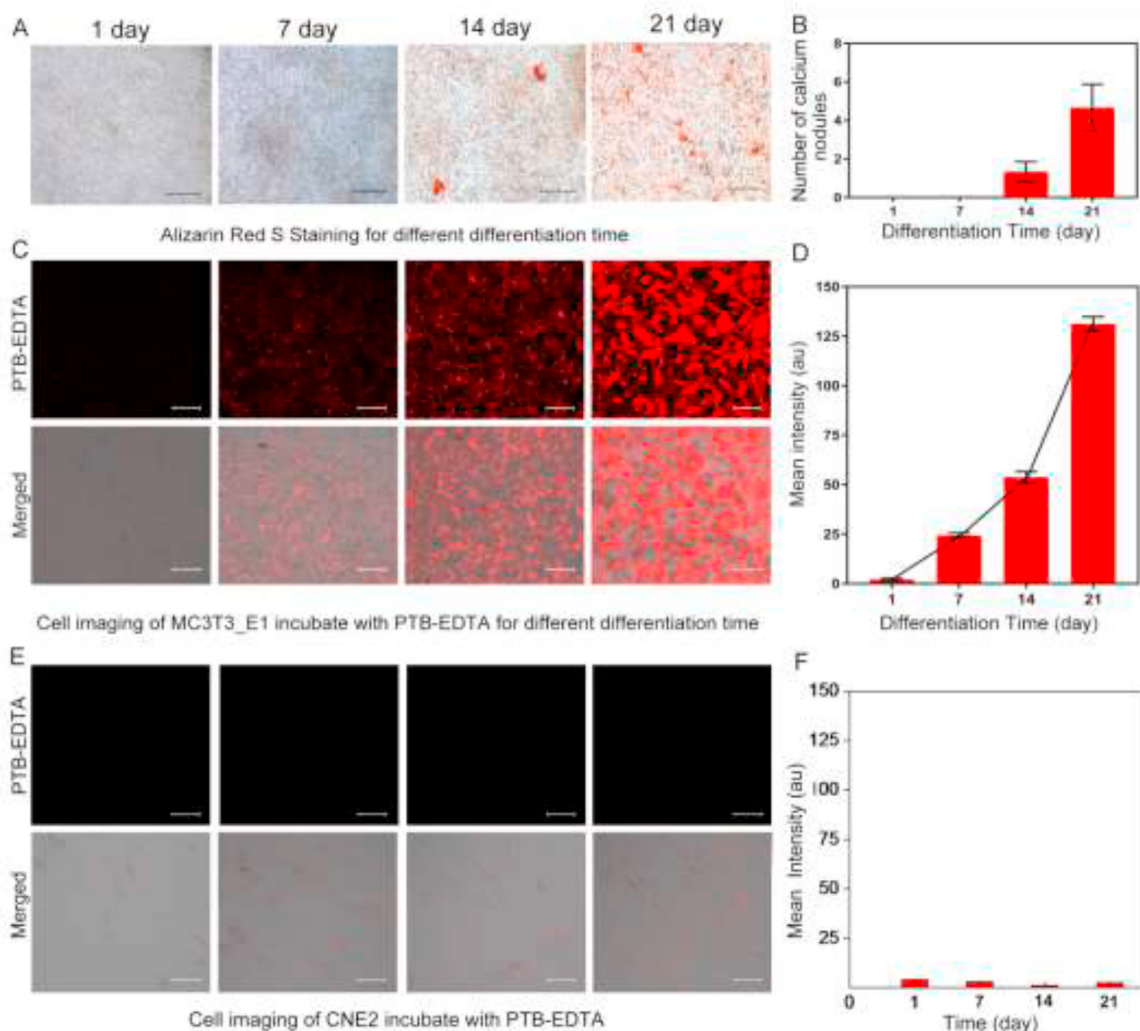


Fig. 4. The fluorescence intensity of PTB-EDTA gradually increased with the osteogenic differentiation. (A) Representative photos of Alizarin Red S staining at indicated differentiation time. Scale bars = 100 μm . (B) Number of mineralized nodules at indicated differentiation time. (C) The fluorescence and merged images of cells incubated with PTB-EDTA for 12 h at indicated differentiation time. (D) Quantification of PTB-EDTA fluorescence intensity at indicated differentiation time. (E) The fluorescence and merged images of CNE2 cells incubated with PTB-EDTA for different times. (F) Quantification of PTB-EDTA fluorescence intensity inside CNE2 cells. Scale bars = 50 μm . PTB-EDTA = 10 μM . (For interpretation of the references to colour in this figure legend, the reader is referred to the Web version of this article.)

high selectivity towards differentiated osteoblasts, making it a high promise to monitor the differentiation process. We proposed that the increasing demand of Ca^{2+} during osteogenic differentiation process played the critical role for the high selectivity [28,29].

The speed and efficacy of cells differentiating into mature osteoblasts and their lifespan determines the rate of bone formation [33]. The use of *in vitro* live cell assays allows real-time monitoring and assessment of cell status, allowing real-time longitudinal assessment of cell responses, which is important in bone research, because *in vitro* studies involve 3 weeks of cell culture to allow for ECM maturation and mineralization. Thus, after verifying its selectivity, we validated the quantification of osteogenic differentiation using PTB-EDTA, fluorescence readouts of this polymer were monitored and compared to the method of Alizarin Red S staining. Fig. 4A shows representative images of Alizarin Red S staining at each time point, and the number of mineralized nodules increased with the elongation of osteogenic differentiation time (Fig. 4B). Meanwhile, as shown in Fig. 4C and D, the intracellular fluorescence intensity of PTB-EDTA increased with slight background fluorescence as the matrix became more mineralized. Whereas, no obvious fluorescence was detected in the undifferentiated

cells (Fig. 4E and F), demonstrating its high selectivity. In addition, fluorescence detection based on PTB-EDTA is more sensitive to osteogenic differentiation than that of Alizarin Red S staining, in which the fluorescence of PTB-EDTA was detectable from the 7th day of differentiation, while mineralized nodules were only apparent from the 14th day with Alizarin Red S staining. Thus, the monitoring of PTB-EDTA fluorescence in osteoblasts can provide a convenient method for detecting the osteogenic differentiation.

Herein, no cell fixation was needed for strategy based on PTB-EDTA compared to Alizarin Red S staining. Thus, the real-time monitoring of differentiation during different stages could be acquired with high selectivity and sensitivity by using PTB-EDTA. In order to observe the advantage of PTB-EDTA compared to low-mass molecules, we further observed the imaging ability of MTB-EDTA (the chemical structure is illustrated in Scheme S1B) towards osteogenically differentiated MC3T3-E1 cells. The results revealed that no obvious fluorescence was detected in MC3T3-E1 cells (Fig. S5), demonstrating that the MTB-EDTA cannot aggregate in cells. These results indicate that PTB-EDTA can be used as a fluorescent probe to detect and monitor osteogenic differentiation *in vitro*.

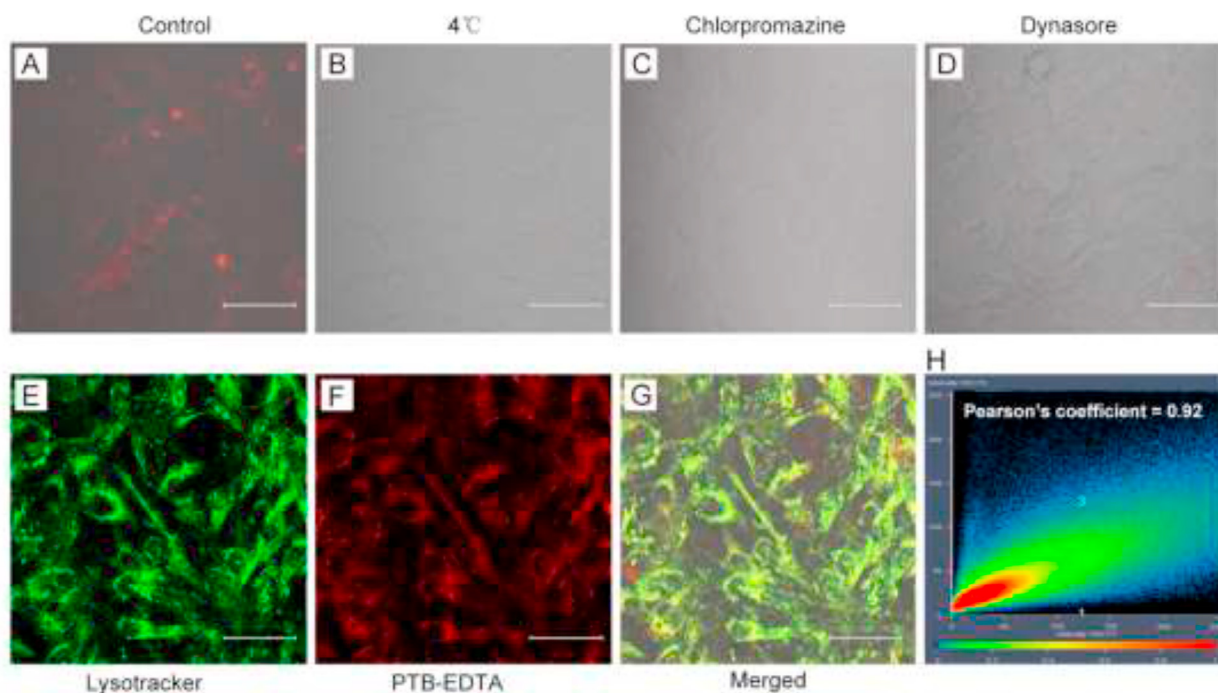


Fig. 5. PTB-EDTA enters the cell lysosome via the endocytic pathway. MC3T3-E1 cells were induced to osteogenic differentiation for 14 days. (A) CLSM images of cells incubated with PTB-EDTA for 6 h in control group; (B) Fluorescence intensity of cells which were incubated with PTB-EDTA at 4 °C for 6 h. (C) CLSM images of cells which were pretreated with chlorpromazine for 30 min, and incubated with PTB-EDTA for 6 h. (D) CLSM images of cells which were pretreated with dynasore for 1 h, and incubated with PTB-EDTA for 6 h. (E) Lysosomal fluorescence distribution in cells. (F) PTB-EDTA fluorescence distribution in cells. (G) The merged images of Lysotracker and PTB-EDTA. (H) Colocalization analysis of Lysotracker and PTB-EDTA. $\lambda_{\text{ex}} = 454 \text{ nm}$ for PTB-EDTA, $\lambda_{\text{ex}} = 543 \text{ nm}$ for Lysotracker. Scale bars = 50 μm . Lysotracker = 100 nM. PTB - EDTA = 20 μM .

3.4. Imaging mechanism investigation

To determine the mechanism of PTB-EDTA for selective imaging towards osteogenically differentiated cells, we investigated its uptake pathway. We observed the imaging ability of PTB-EDTA towards osteogenically differentiated cells under low temperature. Results showed that when the cells were treated under 4 °C, no obvious intracellular fluorescence of PTB-EDTA was found compared with the control group (Fig. 5A and B), indicating that the internalization of PTB-EDTA into cells is energy-dependent. Subsequently, endocytosis inhibitors were used to confirm the endocytic pathway. We found that the fluorescence intensity of intracellular PTB-EDTA dramatically decreased after the treatment of chlorpromazine and dynasore (Fig. 5C and D), which reveals that the uptake of PTB-EDTA is mediated by clathrin-mediated endocytosis.

Next, we explored the localization of PTB-EDTA inside cells. Lysotracker Red DND-99 is a red fluorescent dye that is widely used to label and trace lysosomes in living cells [34]. MC3T3-E1 cells underwent osteogenic differentiation for 14 days were incubated with PTB-EDTA and Lysotracker sequentially. It was found that the PTB-EDTA showed perfect colocalization with Lysotracker with a Pearson's coefficient of 0.92 (Fig. 5E–H). We concluded that PTB-EDTA can across the cell membrane via the endocytic pathway and enriched in the lysosomes.

To further explore the mechanism of PTB-EDTA entering osteoblasts, the differentiated cells (14 days) were incubated in the presence and absence of Ca^{2+} in MEM medium. Results showed that no obvious fluorescence was observed in cells incubated in MEM medium without Ca^{2+} (Fig. S6). Thus, we proposed that during the osteogenic differentiation process, the Ca^{2+} is highly demanded by osteogenic differentiation cells, making the Ca^{2+} -chelated PTB-EDTA could across the cell membrane via endocytosis to localize in lysosome.

Although endocytosis is ubiquitous in many cells, we found no

obvious red fluorescence in the other cell types, which is probably related to receptor-mediated endocytosis [35] or increased need for Ca^{2+} . During osteogenic differentiation induced by numerous factors, the commonality to all processes is that they are all capable of increasing intracellular calcium [28], and it has been recognized that endocytosis can import Ca^{2+} [36,37]. Therefore, we propose that PTB-EDTA chelated with Ca^{2+} may across the cell membrane through endocytosis in the process of osteogenic differentiation, resulting in the gradual accumulation of PTB-EDTA in lysosomes, thus, the fluorescence could be observed. Therefore, the differentiation degree of osteoblasts can be determined by the degree of the internalization of PTB-EDTA, which can be determined by measuring the intracellular fluorescence intensity.

4. Conclusions

In this study, we designed and prepared a novel conjugated polymer with AIE activity for selective monitoring the osteogenic differentiation degree of osteoblasts for the first time. This polymer has good biosafety and shows no effect on the osteogenetic differentiation. Moreover, this polymer can be used to detect the occurrence of osteogenic differentiation earlier than that of Alizarin Red S staining. During the imaging process, the operation is quite simple as the cell fixing and washing are not required, which is quite different from the previously reported fluorescent probes. In summary, this polymer hold great promising be used for the confirmation of osteoblast differentiation ability and the study of osteoblast differentiation-related drug screening.

CRedit authorship contribution statement

Zhenyu Zheng: Investigation, Methodology, Formal analysis, Writing - original draft, Conceptualization, Writing - review & editing. **Taotao Zhou:** Methodology, Data curation, Investigation, Writing -

original draft. **Rong Hu:** Supervision, Project administration, Visualization, Writing - review & editing. **Minjun Huang:** Project administration, Funding acquisition. **Xiang Ao:** Investigation, Resources. **Jun Chu:** Investigation, Data curation. **Tao Jiang:** Resources, Data curation. **Anjun Qin:** Project administration, Writing - review & editing. **Zhongmin Zhang:** Conceptualization, Writing - review & editing.

Declaration of competing interest

The authors declare no conflict of interest.

Acknowledgements

This work was supported by the Natural Science Foundation of Guangdong Province (Grant No. 2019A1515012074).

Appendix A. Supplementary data

Supplementary data to this article can be found online at <https://doi.org/10.1016/j.bioactmat.2020.06.020>.

References

- [1] D.J. Hak, D. Fitzpatrick, J.A. Bishop, J.L. Marsh, S. Tilp, R. Schnettler, H. Simpson, V. Alt, Delayed union and nonunions: epidemiology, clinical issues, and financial aspects, *Injury* 45S2 (2014) S3–S7, <https://doi.org/10.1016/j.injury.2014.04.002>.
- [2] W. Huang, S. Yang, J. Shao, Y.-P. Li, Signaling and transcriptional regulation in osteoblast commitment and differentiation, *Front. Biosci.* 12 (2007) 3068–3092, <https://doi.org/10.2741/2296>.
- [3] Q. Cai, Y. Shi, D. Shan, W. Jia, S. Duan, X. Deng, X. Yang, Osteogenic differentiation of MC3T3-E1 cells on poly(L-lactide)/Fe₃O₄ nanofibers with static magnetic field exposure, *Mater. Biol. Appl.* 55 (2015) 166–173, <https://doi.org/10.1016/j.msec.2015.05.002>.
- [4] A. Daneault, J. Prawitt, V.F. Soulé, V. Coxam, Y. Wittrant, Biological effect of hydrolyzed collagen on bone metabolism, *Crit. Rev. Food. Sci. Nutr.* 57 (2017) 1922–1937, <https://doi.org/10.1080/10408398.2015.1038377>.
- [5] C.A. Gregory, W.G. Gunn, A. Peister, D.J. Prockop, An Alizarin red-based assay of mineralization by adherent cells in culture: comparison with cetylpyridinium chloride extraction, *Anal. Biochem.* 329 (2004) 77–84, <https://doi.org/10.1016/j.ab.2004.02.002>.
- [6] J. Thyberg, Electron microscopic studies on the initial phases of calcification in Guinea pig epiphyseal cartilage, *J. Ultrastruct. Res.* 46 (1974) 206–218, [https://doi.org/10.1016/s0022-5320\(74\)80056-0](https://doi.org/10.1016/s0022-5320(74)80056-0).
- [7] L.N. Wu, Y. Ishikawa, G.R. Sauer, B.R. Genge, F. Mwale, H. Mishima, R.E. Wuthier, Morphological and biochemical characterization of mineralizing primary cultures of avian growth plate chondrocytes: evidence for cellular processing of Ca²⁺ and Pi prior to matrix mineralization, *J. Cell Biochem.* 57 (1995) 218–237, <https://doi.org/10.1002/jcb.240570206>.
- [8] A.D. Hofemeier, H. Hachmeister, C. Pilger, M. Schürmann, J.F.W. Greiner, L. Nolte, H. Sudhoff, C. Kaltschmidt, T. Huser, B. Kaltschmidt, Label-free nonlinear optical microscopy detects early markers for osteogenic differentiation of human stem cells, *Sci. Rep.* 6 (2016) 26716, <https://doi.org/10.1038/srep26716>.
- [9] B.J. Slater, M.D. Kwan, D.M. Gupta, N.J. Panetta, M.T. Longaker, Mesenchymal cells for skeletal tissue engineering, *Expert Opin. Biol. Ther.* 8 (2008) 885–893, <https://doi.org/10.1517/14712598.8.7.885>.
- [10] M.-T. Cheng, H.-W. Yang, T.-H. Chen, O.K.-S. Lee, Modulation of proliferation and differentiation of human anterior cruciate ligament-derived stem cells by different growth factors, *Tissue Eng. Part A* 15 (2009) 3979–3989, <https://doi.org/10.1089/ten.TEA.2009.0172>.
- [11] Y.-R.V. Shih, C.-N. Chen, S.-W. Tsai, Y.-J. Wang, O.K. Lee, Growth of mesenchymal stem cells on electrospun type I collagen nanofibers, *Stem Cells* 24 (2006) 2391–2397, <https://doi.org/10.1634/stemcells.2006-0253>.
- [12] H. Puchtler, S.N. Meloan, M.S. Terry, On the history and mechanism of alizarin and alizarin red S stains for calcium, *J. Histochem. Cytochem.* 17 (1969) 110–124, <https://doi.org/10.1177/17.2.110>.
- [13] L. Macri-Pellizzeri, N.D. Melo, I. Ahmed, D. Grant, B. Scammell, V. Sottile, Live quantitative monitoring of mineral deposition in stem cells using tetracycline hydrochloride, *Tissue Eng. Part C Methods* 24 (2018) 171–178, <https://doi.org/10.1089/ten.TEC.2017.0400>.
- [14] J. Li, W.-Y.-W. Lee, T. Wu, J. Xu, K. Zhang, D.S.H. Wong, R. Li, G. Li, L. Bian, Near-infrared light-triggered release of small molecules for controlled differentiation and long-term tracking of stem cells in vivo using upconversion nanoparticles, *Biomaterials* 110 (2016) 1–10, <https://doi.org/10.1016/j.biomaterials.2016.09.011>.
- [15] J. Li, C.W.T. Leung, D.S.H. Wong, J. Xu, R. Li, Y. Zhao, C.Y.Y. Yung, E. Zhao, B.Z. Tang, L. Bian, Photocontrolled siRNA delivery and biomarker-triggered luminogens of aggregation-induced emission by up-conversion NaYF₄:Yb³⁺,Tm³⁺@SiO₂ nanoparticles for inducing and monitoring stem-cell differentiation, *ACS Appl. Mater. Interfaces* 11 (2019) 22074–22084, <https://doi.org/10.1021/acsami.7b00845>.
- [16] F.-Y. Cao, Y. Long, S.-B. Wang, B. Li, J.-X. Fan, X. Zeng, X.-Z. Zhang, Fluorescence light-up AIE probe for monitoring cellular alkaline phosphatase activity and detecting osteogenic differentiation, *J. Mater. Chem. B* 4 (2016) 4534–4541, <https://doi.org/10.1039/c6tb00828c>.
- [17] H. Lu, K. Wang, B. Liu, M. Wang, M. Huang, Y. Zhang, J. Yang, Systematic oligoaniline-based derivatives: ACQ–AIE conversion with a tunable insertion effect and quantitative fluorescence “turn-on” detection of BSA, *Mater. Chem. Front.* 3 (2019) 331–338, <https://doi.org/10.1039/C8QM00543E>.
- [18] R. Zhan, Y. Pan, P.N. Manghnani, B. Liu, AIE polymers: synthesis, properties, and biological applications, *Macromol. Biosci.* 17 (2017) 1600433, <https://doi.org/10.1002/mabi.201600433>.
- [19] J. Mei, N.L.C. Leung, R.T.K. Kwok, J.W.Y. Lam, B.Z. Tang, Aggregation-induced emission: together we shine, united we soar!, *Chem. Rev.* 115 (2015) 11718–11940, <https://doi.org/10.1021/acs.chemrev.5b00263>.
- [20] J. Zhang, M. Zheng, F. Zhang, B. Xu, W. Tian, Z. Xie, Supramolecular hybrids of AIEgen with carbon dots for noninvasive long-term bioimaging, *Chem. Mater.* 28 (2016) 8825–8833, <https://doi.org/10.1021/acs.chemmater.6b04894>.
- [21] M. Gao, Q. Hu, G. Peng, B.Z. Tang, B. Liu, A fluorescent light-up probe with “AIE + ESIP” characteristics for specific detection of lysosomal esterase, *J. Mater. Chem. B* 2 (2014) 3438–3442, <https://doi.org/10.1039/C4TB00345D>.
- [22] W. Wu, D. Mao, S. Xu, S. Ji, F. Hu, D. Ding, D. Kong, B. Liu, High Performance photosensitizers with aggregation-induced emission for image-guided photodynamic anticancer therapy, *Mater. Horiz.* 4 (2017) 1110–1114, <https://doi.org/10.1039/C7MH00469A>.
- [23] Y. Zhang, X. Huang, W. Liu, G. Zhang, D. Zhang, X. Jiang, Organic nanoparticles formed by aggregation-induced fluorescent molecules for detection of hydrogen sulfide in living cells, *Sci. China Chem.* 59 (2016) 106–113, <https://doi.org/10.1007/s11426-015-5543-2>.
- [24] Z. Wang, C. Wang, Y. Fang, H. Yuan, Y. Quan, Y. Cheng, Color-tunable AIE-active conjugated polymer nanoparticles as drug carriers for self-indicating cancer therapy via intramolecular FRET mechanism, *Polym. Chem.* 9 (2018) 3205–3214, <https://doi.org/10.1039/C8PY00329G>.
- [25] Y. Shan, W. Yao, Z. Liang, L. Zhu, S. Yang, Z. Ruan, Reaction-based AIEE-active conjugated polymer as fluorescent turn on probe for mercury ions with good sensing performance, *Dyes Pigm.* 156 (2018) 1–7, <https://doi.org/10.1016/j.dyepig.2018.03.060>.
- [26] K. Morishima, F. Ishiwari, S. Matsumura, T. Fukushima, M. Shibayama, Mesoscopic structural aspects of Ca²⁺-triggered polymer chain folding of a tetraphenylethene-appended poly(acrylic acid) in relation to its aggregation-induced emission behavior, *Macromolecules* 50 (2017) 5940–5945, <https://doi.org/10.1021/acs.macromol.7b00883>.
- [27] T. Zhou, R. Hu, L. Wang, Y. Qiu, G. Zhang, Q. Deng, H. Zhang, P. Yin, B. Situ, C. Zhan, A. Qin, B.Z. Tang, An AIE-active conjugated polymer with high ROS-generation ability and biocompatibility for efficient photodynamic therapy of bacterial infections, *Angew. Chem. Int. Ed.* 59 (2020), <https://doi.org/10.1002/ange.201916704>.
- [28] M. Zayzafoon, Calcium/calmodulin signaling controls osteoblast growth and differentiation, *J. Cell. Biochem.* 97 (2006) 56–70, <https://doi.org/10.1002/jcb.20675>.
- [29] L. Petecchia, F. Sbrana, R. Utzeri, M. Vercellino, C. Usai, L. Visai, M. Vassalli, P. Gavazzo, Electro-magnetic field promotes osteogenic differentiation of BM-hMSCs through a selective action on Ca²⁺-related mechanisms, *Sci. Rep.* 5 (2015) 13856, <https://doi.org/10.1038/srep13856>.
- [30] Z. Qiu, X. Liu, J.W.Y. Lam, B.Z. Tang, The marriage of aggregation-induced emission with polymer science, *Macromol. Rapid Commun.* 40 (2018) e1800568, <https://doi.org/10.1002/marc.201800568>.
- [31] D. Wang, K. Christensen, K. Chawla, G. Xiao, P.H. Krebsbach, R.T. Franceschi, Isolation and characterization of MC3T3-E1 preosteoblast subclones with distinct in vitro and in vivo differentiation/mineralization potential, *J. Bone Miner. Res.* 14 (1999) 893–903, <https://doi.org/10.1359/jbmr.1999.14.6.893>.
- [32] L.D. Quarles, D.A. Yohay, L.W. Lever, R. Caton, R.J. Wenstrup, Distinct proliferative and differentiated stages of murine MC3T3-E1 cells in culture: an in vitro model of osteoblast development, *J. Bone Miner. Res.* 7 (1992) 683–692, <https://doi.org/10.1002/jbmr.5650070613>.
- [33] T.D. Rachner, S. Khosla, L.C. Hofbauer, Osteoporosis: now and the future, *Lancet* 377 (2011) 1276–1287, [https://doi.org/10.1016/S0140-6736\(10\)62349-5](https://doi.org/10.1016/S0140-6736(10)62349-5).
- [34] F. Fan, S. Nie, D. Yang, M. Luo, H. Shi, Y.-H. Zhang, Labeling lysosomes and tracking lysosome-dependent apoptosis with a cell-permeable activity-based probe, *Bioconjug. Chem.* 23 (2012) 1309–1317, <https://doi.org/10.1021/bc300143p>.
- [35] A.P. Reyes-Ibarra, A. García-Regalado, I. Ramírez-Rangel, A.L. Esparza-Silva, M. Valadez-Sánchez, J. Vázquez-Prado, G. Reyes-Cruz, Calcium-sensing receptor endocytosis links extracellular calcium signaling to parathyroid hormone-related peptide secretion via a rab11a-dependent and AMSH-sensitive mechanism, *Mol. Endocrinol.* 21 (2007) 1394–1407, <https://doi.org/10.1210/me.2006-0523>.
- [36] J.V. Gerasimenko, A.V. Tepikin, O.H. Petersen, O.V. Gerasimenko, Calcium uptake via endocytosis with rapid release from acidifying endosomes, *Curr. Biol.* 8 (1998) 1335–1338, [https://doi.org/10.1016/S0969-9822\(07\)00565-9](https://doi.org/10.1016/S0969-9822(07)00565-9).
- [37] T. Pozzan, R. Rizzuto, P. Volpe, J. Meldolesi, Molecular and cellular physiology of intracellular calcium stores, *Physiol. Rev.* 74 (1994) 595–636, <https://doi.org/10.1152/physrev.1994.74.3.595>.